Theoretical study on the excitation spectrum and the photofragmentation reaction of $Ni(CO)_4$

M. Hada, Y. Imai, M. Hidaka, and H. Nakatsuji[a)]
Department of Synthetic and Biological Chemistry, Faculty of Engineering, Kyoto University, Sakyo-ku, Kyoto, 606, Japan

(Received 11 April 1995; accepted 12 July 1995)

The ground and excited states of $Ni(CO)_4$ are studied using the symmetry adapted cluster (SAC)/SAC-configuration interaction (SAC-CI) method. The experimental absorption spectrum is well reproduced by the present calculations. All the peaks observed in the range of 200~350 nm are assigned to the electronic allowed $^1T_2$ excited states. The third peak is assigned to the $3\,^1T_2$ and $4\,^1T_2$ states. Next, the potential energy curves of the ground and the low-lying excited states are calculated by the same method and utilized to clarify the mechanism of the photofragmentation reaction of $Ni(CO)_4$ by a XeCl laser (308 nm). A reaction pathway involving several excited states is proposed for the photofragmentation reaction into the excited $Ni(CO)_3$ and CO. The calculated emission energy from the former agrees well with the observed luminescence spectrum. © *1995 American Institute of Physics.*

I. INTRODUCTION

Transition-metal carbonyls have some importance in laser chemistry as sources of metal atoms or as precursors for chemical vapor deposition (CVD) on thin films.[1,2] The knowledge on the excited states of these compounds and their decay channels are valuable to design and control the laser-induced CVD.

$Ni(CO)_4$ shows a typical photofragmentation reaction and there are much experimental investigations so far, while theoretical investigations based on *ab-initio* molecular orbital methods are very few.[3] The observed absorption spectrum of $Ni(CO)_4$[4] has been assigned only by using the CNDO-CI method[5] and the INDO/S method,[6] but their assignments are not consistent. Reliable assignments based on an accurate theory is necessary.

In the photofragmentation reaction of $Ni(CO)_4$, the excited states of $Ni(CO)_n$ ($n=0$ to 3) are observed by the spectroscopic methods.[7–9] In particular, Rösch *et al.* reported from the experiment using the XeCl laser (308 nm) that $Ni(CO)_4$ dissociates into CO and the excited $Ni(CO)_3^*$ and the strong emission around 650 nm follows the reaction.[7] They proposed the following mechanism for this reaction based on the calculations using the *ab-initio* $X\alpha$ method:[3,7]

$$Ni(CO)_4 + h\nu(308\ \text{nm}) \rightarrow Ni(CO)_4^*,$$

$$Ni(CO)_4^* \rightarrow Ni(CO)_3^* + CO,$$

$$Ni(CO)_3^* \rightarrow Ni(CO)_3 + h\nu(\text{around } 650\ \text{nm}).$$

$Ni(CO)_4$ is excited to the $^1T_2$ state and dissociates into $Ni(CO)_3^*$ and CO. The excited $Ni(CO)_3^*$ exhibits a emission spectrum around 650 nm. This mechanism should be examined by calculating the potential energy surfaces of the low-lying excited states.

In this paper, we investigate the ground and excited states of $Ni(CO)_4$ and assign the peaks on the uv absorption spectrum. After confirming the accuracy of our calculations, we discuss the mechanism of the photofragmentation reaction involving the excited states. We use the symmetry adapted cluster expansion (SAC)[10] and SAC-CI[11] methods, which have been applied successfully to the spectroscopies and the reactions of a number of molecules including transition-metal complexes.[12–14]

II. METHOD OF CALCULATIONS

We employ the basis sets proposed by Huzinaga *et al.*[15] $(14s8p5d)/[6s2p2d]$ set augmented with two polarization p functions ($\zeta=0.049$, 0.153) for Ni, $(9s5p)/[4s2p]$ set with the Rydberg $s(\zeta=0.032)$ and $p(\zeta=0.028)$ functions for C, and $(9s5p)/[4s2p]$ set with the Rydberg $s(\zeta=0.023)$ and $p(\zeta=0.021)$ functions for O.

The Hartree–Fock (HF) calculations are carried out using the HONDO8 program.[16] The electron correlations involved in the ground state are taken into account by the SAC theory and those in the excited states by the SAC-CI theory. The calculations are carried out with the use of the modified version of SAC85.[17] The active space in the SAC/SAC-CI calculations involves 21 occupied orbitals and 44 unoccupied orbitals for $Ni(CO)_4$, 17 occupied orbitals and 35 unoccupied orbitals for $Ni(CO)_3$. To reduce the number of configurations, the configuration selection technique based on the second order perturbation method[18] is used with the thresholds of 2×10^{-5} and 5×10^{-5} for the ground and excited states, respectively. The numbers of the linked operators involved in the ground state are around 2900 for $Ni(CO)_4$ and 2300 for $Ni(CO)_3$. Those involved in the excited states are around 24 500 for $Ni(CO)_4$ and 24 000 for $Ni(CO)_3$.

For the calculations of the excitation spectrum of $Ni(CO)_4$, we use the experimental geometrical parameters.[19] For drawing the potential energy curves, we optimize the geometry of $Ni(CO)_4$ by the HF method, and use it as the initial structure. The Ni–CO distance is elongated with fixing $Ni(CO)_3$ and CO. For the calculations of the emission energy of the excited $Ni(CO)_3^*$, the geometry is optimized by the

[a)]Also belongs to the Institute for Fundamental Chemistry, 34-4 Takano Nishi-Hiraki-cho, Sakyo-ku, Kyoto, 606, Japan.

TABLE I. Experimental and optimized geometrical parameters of $Ni(CO)_4$, $Ni(CO)_3$, and CO in the ground state (Å).

		Experimental		Optimized	
Fragment	Symmetry	R_{Ni-C}	R_{C-O}	R_{Ni-C}	R_{C-O}
$Ni(CO)_4$	T_d	1.838[a]	1.141[a]	1.864	1.139
$Ni(CO)_3$	D_{3h}			1.820	1.141
Free CO	$C_{\infty v}$		1.1283[b]		1.136

[a]Reference 19.
[b]K. P. Huber and G. Herzberg, *Molecular Spectra and Molecular Structure*, Vol. 4 (Van Nostrand, Princeton, 1979).

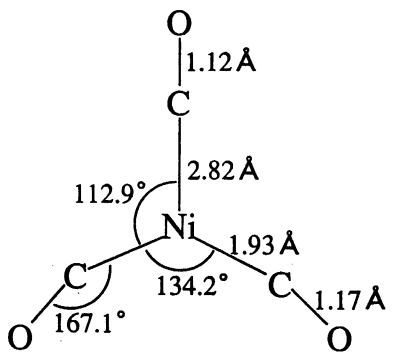

FIG. 1. Optimized geometry of $Ni(CO)_3$ in the first excited state $1B_1$. The molecular symmetry is C_{2v}.

single-excitation CI (SECI) method. The geometry of $Ni(CO)_3$ in the ground state is also optimized by the HF method for comparison. The program used for these optimizations is GAUSSIAN92.[20] The geometrical parameters obtained and used in our calculations are summarized in Table I and Fig. 1.

III. EXCITATION SPECTRUM OF $Ni(CO)_4$

To characterize the excited states of $Ni(CO)_4$, we show in Table II the HF molecular orbitals of $Ni(CO)_4$ employed in the SAC/SAC-CI calculations. The basic bonding character involved in the ground state of $Ni(CO)_4$ has been well studied.[21–24] The $8t_2$ and $9t_2$ orbitals have the Ni–CO bonding character. The highest occupied $2e$ and $9t_2$ orbitals are mainly composed of the Ni $3d$ orbitals, and the lower $8t_2$ and $8a_1$ orbitals are essentially the CO 5σ MOs. The unoccupied $12t_2$, $4e$, and $13t_2$ MOs are the antibonding orbitals between the metal $3d$ and CO π^* orbitals, and they play an important role in the low-lying excited states. The Hartree–Fock energy is −1957.096 287 a.u., and the electron correlation energy calculated by the SAC method is −0.263 627 a.u. for the ground state.

TABLE II. Orbital energies and the characters of the Hartree–Fock SCF orbitals of $Ni(CO)_4$.

Orbital energy (eV)	Orbital symmetry	Nature[a]
−22.56	$7a_1$	CO 4σ
−22.03	$6t_2$	CO 4σ
−19.00	$8a_1$	CO 5σ
−18.09	$1e$	CO π
−18.00	$7t_2$	CO π
−17.74	$1t_1$	CO π
−17.48	$8t_2$	CO 5σ+Ni $3dxz,yz,x^2-y^2$
−12.64	$2e$	Ni $3dz^2,xy$
−10.46	$9t_2$	Ni $3dxz,yz,x^2-y^2,4p$+CO π^*
0.60	$9a_1$	Ni $4s$, CO Ryd. sp
0.81	$10t_2$	CO Ryd. sp
1.46	$11t_2$	CO Ryd. sp
1.52	$3e$	Co Ryd. p
1.97	$2t_1$	CO Ryd. p
2.25	$10a_1$	Ni $4s$, CO Ryd. p
2.33	$12t_2$	Ni $3dxz,yz,x^2-y^2,4p$−CO π^*, CO Ryd. sp
2.86	$4e$	Ni $3dz^2,xy$−CO π^*, CO Ryd. sp
3.01	$13t_2$	Ni $3dxz,yz,x^2-y^2,4p$−CO π^*, 5σ,Ni $4p$, CO Ryd. sp
3.10	$11a_1$	Ni $4s$, CO Ryd. sp
3.38	$14t_2$	Ni $3d$−CO π^*, 5σ, CO Ryd. sp
3.75	$3t_1$	CO π^*, CO Ryd. p
3.80	$15t_2$	Ni $4p$, CO Ryd. p
4.01	$5e$	CO π^*, CO Ryd. p
4.71	$4t_1$	CO π^*, CO Ryd. p
4.97	$12a_1$	Ni $4s$, CO σ^*, CO Ryd. sp
5.47	$16t_2$	Ni $4p$, CO σ^*, CO Ryd. sp
6.86	$13a_1$	Ni $4s$, Ni $3s$−CO 5σ, CO Ryd. p
7.83	$17t_2$	Ni $4p$, CO π^*, CO Ryd. sp

[a]Plus (+) and minus (−) signs mean bonding and antibonding characters.

The excitation energies, intensities, and their assignments are summarized in Table III. The transitions from the ground state to the T_2 states are optically allowed, and four T_2 states are found to exist in the range of 4~6.5 eV.

In Fig. 2, the absorption spectrum of $Ni(CO)_4$ observed by Rösch *et al.*[4] is compared with the present excitation energies and their intensities. The SAC-CI results show a good agreement with the experimental spectrum. The calculated intensities are natural compared with the experiment. The first T_2 state appearing at ~260 nm (4.7 eV) is assigned to the shoulder of the experimental absorption spectrum. The SECI calculation can not reproduce the experimental spectrum particularly in the energy region higher than 5.2 eV (~240 nm).

All the peaks observed in the range of 200~350 nm (6.2~3.5 eV) are reasonably assigned to the dipole allowed $^1T_2$ excited states. The third peak in the experimental spectrum is assigned to the $3T_2$ and $4T_2$ states as shown in Table III, because they are separated only by 0.04 eV. The excitation energies of $2T_2$~$4T_2$ calculated by the SECI method are too high compared with the experimental values, while those calculated by the INDO/S-CI method are much lower than the experimental values. The order of the excitation energies calculated by the SAC-CI method is different from those calculated by the SECI and INDO/S-CI methods. For example, the characters of the $3T_2$ and $4T_2$ states in the SECI calculations correspond to those of $4T_2$ and $3T_2$, respectively, in the SAC-CI calculations. In the $X\alpha$ calculation,[3] the excitation energy of the $1T_2$ state is calculated to be 4.88 eV, which reasonably agrees with the experiments, though there are no assignments for the other observed peaks.

The above results show that our calculations are reliable

TABLE III. Excitation energies and oscillator strengths of $Ni(CO)_4$ calculated by the SECI and the SAC-CI methods compared with the previous theoretical and experimental results.

State	Main configurations[a]	SAC-CI		Excitation energy (eV)			
		Excitation energy (eV)	Oscillator strength	Expt.	SECI	$X\alpha$[c]	INDO/S[b]
$1E$	$0.56(9t_2\rightarrow 12t_2)$	4.52	Forbidden		4.77		3.98
$1T_1$	$0.62(9t_2\rightarrow 12t_2)$	4.53	Forbidden		4.58		3.93
$1T_2$	$0.54(9t_2\rightarrow 12t_2),0.08(9t_2\rightarrow 4e)$	4.79	2.3×10^{-2}	4.6	4.99	4.88[e]	4.15
$2T_1$	$0.78(9t_2\rightarrow 4e),0.11(9t_2\rightarrow 3e)$	4.97	Forbidden		5.38		4.05
$3T_1$	$0.59(2e\rightarrow 12t_2),0.11(2e\rightarrow 13t_2)$	5.25	Forbidden		6.00		4.55
$2A_1$	$0.43(2e\rightarrow 4e),0.28(9t_2\rightarrow 12t_2)$	5.41	Forbidden		5.99		4.56
$2T_2$	$0.48(9t_2\rightarrow 4e),0.18(2e\rightarrow 12t_2)$ $0.20(9t_2\rightarrow 9a_1)$	5.51	6.7×10^{-2}	5.4	6.34		4.36
$3T_2$	$0.69(9t_2\rightarrow 9a_1),0.20(9t_2\rightarrow 10a_1)$ $0.10(9t_2\rightarrow 3e)$	5.72	4.3×10^{-2}	6.0	7.68[d]		4.39
$4T_2$	$0.42(2e\rightarrow 12t_2),0.19(9t_2\rightarrow 3t_1)$	5.76	8.9×10^{-2}		6.58[d]		4.91
$1A_2$	$0.57(2e\rightarrow 4e),0.25(9t_2\rightarrow 3t_1)$	6.07	Forbidden		7.07		4.64
$2E$	$0.24(9t_2\rightarrow 10t_2),0.42(2e\rightarrow 4e),$ $0.23(9t_2\rightarrow 3t_1)$	6.28	Forbidden		7.41		4.79

[a]Configurations whose square of the coefficients are larger than 0.08 in the SAC-CI results are given.
[b]Reference 6.
[c]Reference 3.
[d]The characters of the $3T_2$ and $4T_2$ states in the SECI calculations correspond to those of the $4T_2$ and $3T_2$ states in the SAC-CI calculations.
[e]This value is taken from Fig. 5 in Ref. 9.

enough to discuss the photofragmentation reaction mechanism in some details.

The characters of the low-lying excited states are as follows. The main configurations for the $1T_2$ and $2T_2$ states are the excitations, $9t_2\rightarrow 12t_2$ and $9t_2\rightarrow 4e$, respectively, and both are assigned to Ni $3d\rightarrow$CO π^*. In these states the Ni–CO bonding is weakened. The $3T_2$ state involves the excitation within the metal, and the $4T_2$ state is again assigned to Ni $3d\rightarrow$CO π^*. Invisible low-lying states $1E$ and $1T_1$ exist below the $1T_2$ state and both are characterized as $9t_2\rightarrow 12t_2$. This $1T_1$ state plays an important role in the photofragmentation reaction, as discussed below.

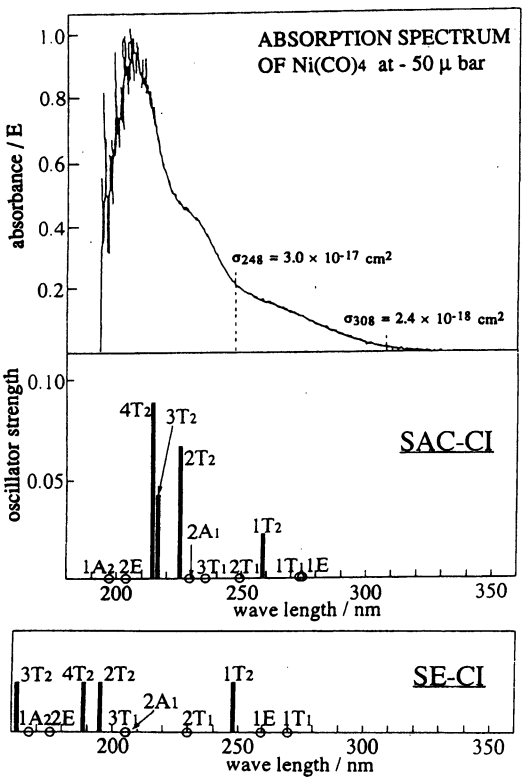

FIG. 2. Comparison between experimental and theoretical absorption spectra.

IV. PHOTOFRAGMENTATION REACTION BY 308 nm LASER

A. Dissociation from the $1T_2$ state

As seen from the experimental absorption spectrum of $Ni(CO)_4$ shown in Fig. 2, the uv irradiation at 308 nm, which is at the tail of the lowest absorption peak, would produce the lowest allowed $1T_2$ state. Considering the bonding characters in the $1T_2$ state described above, the Ni–CO bonding is weakened in the excited state. Further, the Jahn–Teller distortion should occur in the T_2 state. To make clear what happens in this situation, we draw the potential energy curves for the ground and low-lying excited states as a function of the Ni–CO distance, and the results are shown in Fig. 3. The potential curves on the left-hand side were calculated by the SECI method and those on the right-hand side by the SAC-CI method. The geometries of $Ni(CO)_3$ and CO are fixed in this figure.

First, we compare the SAC-CI results with the SECI results. These two methods give some different results for the $2A_1$ and $3E$ states, which are derived from the $1T_2$ state in the T_d symmetry. Both $2A_1$ and $3E$ states calculated by the SECI method have attractive potential curves, while the $2A_1$ state calculated by the SAC-CI method has a repulsive potential. The $2A_1$ state becomes lower than the $2E$ state. Considering the bonding character involved in the $2A_1$ state,

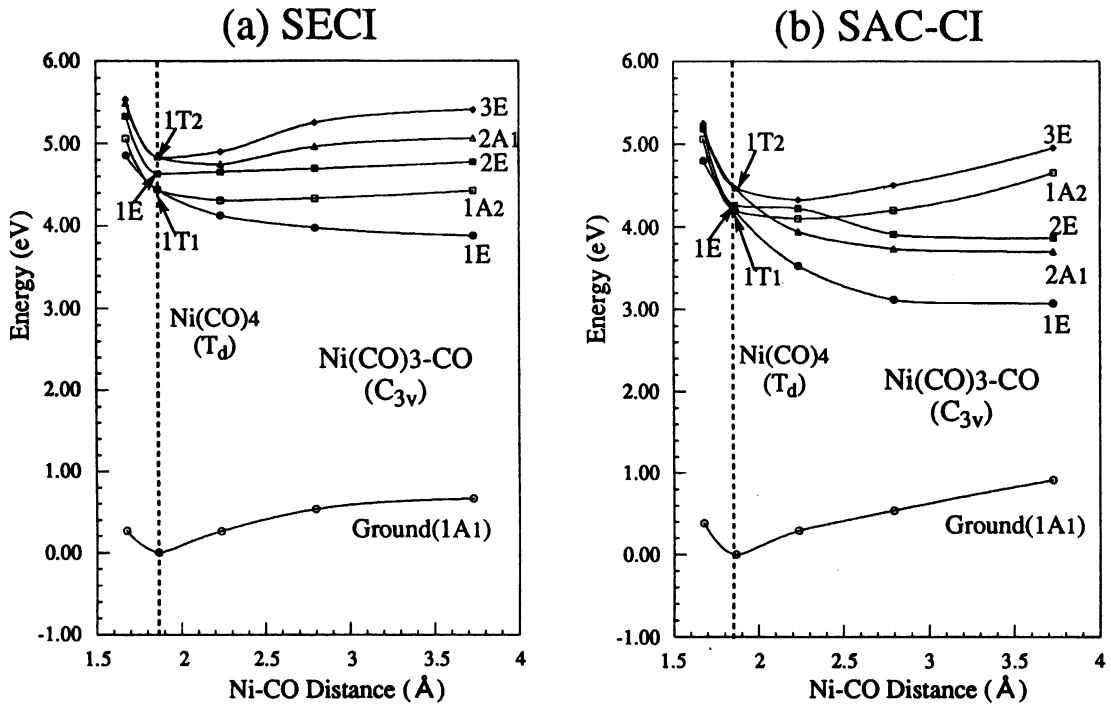

FIG. 3. Potential energy curves for the dissociation of CO from $Ni(CO)_4$ calculated by (a) the SECI method and (b) the SAC-CI method.

the repulsive character of this potential is reasonable. In the following discussion, we use only the SAC-CI results shown in Fig. 3(b), since they are more reliable as shown in the above section.

In the $1T_2$ excited state, $Ni(CO)_4$ would be distorted by the Jahn–Teller effect. The Ni–CO stretching would be allowed to couple with the electronic T_2 state and therefore one CO ligand starts to dissociate along the repulsive potential curve of the $2A_1$ state as shown in Fig. 3(b). The $3E$ state does not give a repulsive curve as shown in Fig. 3(b). Figure 4 shows the overall energy diagram along the photodissociation path.

The $1E$ state exists below of the $2A_1$ state as the lowest state throughout this reaction pathway as shown in Fig. 3(b). The $[Ni(CO)_3–CO]^*$ species on the potential curve of the $2A_1$ state is supposed to relax to this lowest excited state $1E$ by the internal conversion, as described in the Kasha's rule.[25] As the potential curve of the $1E$ state is more repulsive than that of the $2A_1$ state, the $[Ni(CO)_3–CO]^*$ system would dissociate completely along this repulsive potential curve. At the dissociation limit, the curve leads to the excited state $Ni(CO)_3$ and the ground state CO. This result suggests that the dissociated CO is excited mainly translationally and vibrationally, and not rotationally, as analyzed by Schlenker *et al.*[26]

We note here that Rösch *et al.* have pointed out that the $1E$ state of $[Ni(CO)_3–CO]$ species derived from the $1T_2$ state of $Ni(CO)_4$ plays an important role in the photodissociation process,[3] though the $1T_2$ state of $Ni(CO)_4$ does not give the $1E$ state but gives the $2E$ or $3E$ state in our calculations, as shown in Fig. 3(b).

There is another possibility that $Ni(CO)_4$ is excited directly to the $1T_1$ state, which is lower than the $1T_2$ state, by the 308 nm laser, though this transition is dipole forbidden. In this case, $Ni(CO)_4$ dissociates into $Ni(CO)_3^*$ and CO along the $1E$ potential curve without the internal conversion. Therefore, this reaction path gives the same species as that involving the $1T_2$ state described above.

B. Geometrical relaxation in the excited state of $Ni(CO)_3$

The excited intermediate $[Ni(CO)_3–CO]^*$ relaxes from the $2A_1$ state to the $1E$ state, as described above. In this $1E$ state, the geometry of $Ni(CO)_3$ is again distorted by the Jahn–Teller effect, and the $1E$ state is separated into the A' and A'' states in the C_s symmetry. Assuming that this geometrical relaxation occurs after the dissociation of the system into $Ni(CO)_3$ and CO, we optimized the geometry of $Ni(CO)_3$ in the lowest excited $2A'$ state at the SECI level. The $Ni(CO)_3^*$ fragment in this excited state relaxes from a nonplanar structure (C_{3v}) to a planar one (C_{2v}) by this optimization, as shown in Fig. 1. The stable geometry of $Ni(CO)_3$ in the ground state is a planar regular triangle (D_{3h}).

Here, we discuss the relationship between the geometry of $Ni(CO)_3$ and the electronic state $1E$. In the planar regular triangle D_{3h} form, the lowest excited state $1E''$ corresponds

to the excitation from the HOMO $9e'(Ni3d_{xy,x^2-y^2})$ to the LUMO $4a''(Ni4p_z+CO\pi^*)$ shown below.

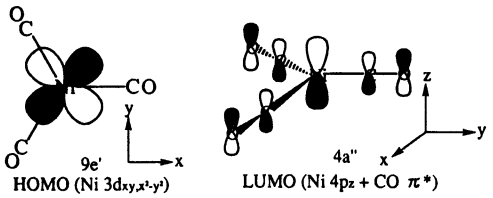

In this excited state, the electronic structure is degenerate ($1E$), so that the geometry is distorted by the Jahn–Teller effect and becomes the structure shown in Fig. 1, which is the SECI optimized geometry. Furthermore, since the $4a''$ orbital possesses the bonding character between Ni and CO, we expect that the spontaneous dissociation of the second CO ligand would not occur from this state.

Thus the geometry of $Ni(CO)_3$ is much relaxed when $Ni(CO)_4$ dissociates photochemically into $Ni(CO)_3^*$ and CO. As shown in Fig. 1, the optimized geometry of the excited $Ni(CO)_3$ in the C_{2v} symmetry is much different from that of the ground state $Ni(CO)_4$ in the T_d symmetry. Considering this large relaxation, we expect that the vibrational mode of $Ni(CO)_3^*$ is excited, as well as the vibrational and translational modes of the dissociated CO.

C. Overall reaction mechanism and the nature of the luminescence

We here summarize the mechanism of the photolysis of $Ni(CO)_4$ into $Ni(CO)_3$ and CO described above, and investigate the nature of the luminescence which follows the photolysis.

Figure 4 shows the overall energy diagram along the dissociation path. From the results of the previous sections, the overall reaction mechanism of the photolysis of $Ni(CO)_4$ may be summarized as follows. $Ni(CO)_4$ which is excited to the allowed $1T_2$ state by the XeCl laser is distorted by the Jahn–Teller effect, the Ni–CO elongation path couples with this distortion mode, and one carbonyl ligand dissociates along the repulsive potential curve of the $2A_1$ state originating from the $1T_2$ state. Then, the excited system $[Ni(CO)_3–CO]^*$ is relaxed, by the internal conversion, to the lowest excited state $1E$ originating from the $1T_1$ state, but since this state is degenerate, it is again distorted by the Jahn–Teller effect, and led to the repulsive $2A'$ potential, and finally dissociates into the excited $Ni(CO)_3^*$ and the ground state CO molecule. Of course, the two step Jahn–Teller distortions described above may occur in one step.

The luminescence spectrum which follows the photolysis of $Ni(CO)_4$ with 308 nm laser was first observed and analyzed by Rösch *et al.*[7] Afterwards, it was observed and investigated more precisely by several authors[8,9] and assigned to be due to the transition from the excited state $Ni(CO)_3^*$, which is the photolysis product, to its ground state. In Table IV, the transition energy and the oscillator strength calculated by the SAC-CI method are compared with the experimental data. As the geometry was optimized in the excited $1B_1$ state (C_{2v}), the transition energy is regarded as the emission energy from the $1B_1$ state to the ground state, and therefore can be compared with the observed luminescence. The calculated luminescence energy 1.54 eV agrees well with the maximum emission energies 1.7~2.0 eV of the observed luminescence spectra. The vertical excitation energy of $Ni(CO)_3$ from the ground state geometry (D_{3h}) is 2.58 eV, which is larger than the emission energy by about 1 eV. This shows that the emission energy changes considerably by the geometrical change of $Ni(CO)_3$.

TABLE IV. The first excited state of $Ni(CO)_3$ in the D_{3h} and C_s symmetries compared with the energies of the luminescence.

Symmetry	Luminescence energy (eV)	Configurations[c]	Oscillator strength
$1E''(D_{3h})$[a]	2.58	$0.72(9e'\rightarrow 4a'')$[d] $0.18(9e'\rightarrow 5a'')$[d]	Forbidden
$1B_1(C_{2v})$[b]	1.54	$0.62(18a_1\rightarrow 6b_1)$[d] $0.11(18a_1\rightarrow 8b_1)$[d] $0.10(18a_1\rightarrow 7b_1)$[d]	1.07×10^{-3}
Expt.[e]	1.5~2.3[f](1.9) 1.4~2.4[g](1.7) 1.7~2.4[h](2.0)		

[a]The geometry is optimized for the ground state.
[b]The geometry is optimized for the excited $1B_1$ state.
[c]Configurations whose square of the coefficients are larger than 0.08 in the SAC-CI results are given.
[d]$9e'$ is Ni $3d_{xy,x^2-y^2}$, and $4a''$ and $5a''$ are both Ni $4p_z$+CO π^*. $18a_1$ is Ni $3d_{x^2-y^2}$, and $6b_1$, $7b_1$, and $8b_1$ are all $4p$+CO π^*.
[e]These values are taken from the luminescence spectra. The values in parentheses show the maximum peak positions in the spectra.
[f]Reference 6.
[g]Reference 7.
[h]Reference 8.

Two features are remarkable in the experimental luminescence spectra, namely the broadness (about 0.8 eV) and the long lifetime (>10 μs). The long lifetime may be explained by the small value of the oscillator strength, 1×10^{-3} calculated by the SAC-CI method, because this transition is originally forbidden in the D_{3h} symmetry. The broadness of the spectrum would be attributed to the facts that in the excited state, the vibrational levels of $Ni(CO)_3^*$ should be high and that the geometries of the ground and excited states are largely different.

V. CONCLUSION

The electronic excitation spectrum and the photofragmentation reaction of $Ni(CO)_4$ with the 308 nm laser have been investigated theoretically using the SAC/SAC-CI method. The results may be summarized as follows.

(1) The calculated excitation energies and the oscillator strengths of $Ni(CO)_4$ show a good agreement with the experimental absorption spectrum. All the observed peaks are assigned as being due to the excitations to the allowed T_2 states. The observed third peak is assigned to the $3T_2$ and $4T_2$ states.

(2) The mechanism of the photofragmentation reaction and the luminescence is illustrated in Fig. 4 and may be summarized as follows. First, $Ni(CO)_4$ is excited to the allowed $1T_2$ state by the 308 nm laser. The geometry of $Ni(CO)_4^*$ in the $1T_2$ state is distorted along the repulsive potential of the $2A_1$ state. This $[Ni(CO)_3–CO]^*$ species

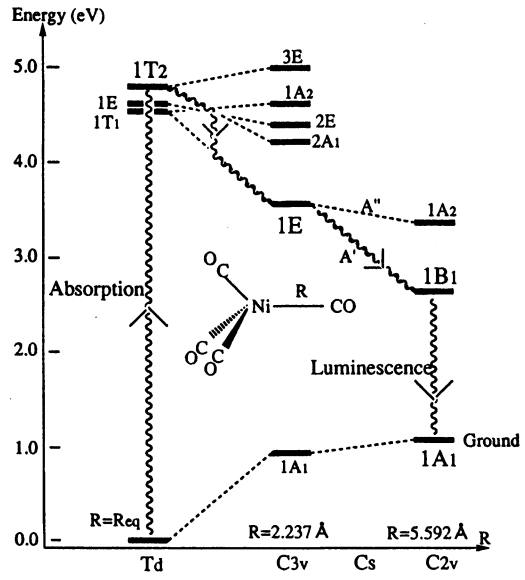

FIG. 4. Overall energy diagram and the pathway for the photofragmentation reaction of $Ni(CO)_4$.

makes an internal conversion to the lowest excited state $1E$, as the Kasha's rule implies. In this $1E$ state, the species $[Ni(CO)_3–CO]^*$ is further distorted and led to the $1B_1$ excited state of $Ni(CO)_3$ and the ground state CO. The excited $Ni(CO)_3^*$ gives a luminescence and de-excited to the ground state.

(3) Since Ni–CO is bonding in these excited states, further CO dissociation does not occur in this process.

(4) The calculated emission energy from the excited $1B_1$ state of $Ni(CO)_3$ agrees well with the luminescence spectrum.

When higher energy is supplied, the products $Ni(CO)_2$, Ni(CO), and Ni are observed in the $Ni(CO)_4$ photolysis,[9,26] and the luminescence spectra from these species are observed.[9] We are currently studying the mechanisms of these reactions using the SAC-CI method.

ACKNOWLEDGMENTS

A part of the calculations has been carried out with use of the computers at the Computer Center at the Institute for Molecular Science. This study has partially been supported by the Grant-in-Aid for Scientific Research from the Ministry of Education, Science, and Culture.

[1] D. J. Ehrlich and J. Y. Tsao, J. Vac. Sci. Technol. B **1**, 969 (1983).
[2] S. Boughaba and G. Auvert, Appl. Surf. Sci. **69**, 79 (1993).
[3] N. Rösch, H. Jörg, and M. Kotzian, J. Chem. Phys. **86**, 4038 (1987).
[4] H. Schröder, B. Rager, S. Metev, N. Rösch, and H. Jörg, in *Interfaces Under Laser Irradiation*, NATO ASI-Series Ser. E (Nijhoff, Dordrecht, 1987), pp. 255–276.
[5] B. Dick, H.-J. Freund, and G. Hohlneicher, Mol. Phys. **45**, 427 (1982).
[6] M. Kotzian, N. Rösch, H. Schröder, and M. C. Zerner, J. Am. Chem. Soc. **111**, 7687 (1989).
[7] N. Rösch, M. Kotzian, and H. Jörg, J. Am. Chem. Soc. **108**, 4238 (1986).
[8] D. M. Preston and J. I. Zink, J. Phys. Chem. **91**, 5003 (1987).
[9] H. Reiner, Ch. Wittenzellner, H. Schröder, and K. L. Kompa, Chem. Phys. Lett. **195**, 169 (1992).
[10] H. Nakatsuji and K. Hirao, J. Chem. Phys. **68**, 2053 (1978).
[11] H. Nakatsuji, Chem. Phys. Lett. **59**, 362 (1978); **67**, 329 (1979).
[12] H. Nakatsuji, Acta. Chim. Hungarica. **129**, 719 (1992).
[13] (a) H. Nakatsuji and S. Saito, J. Chem. Phys. **93**, 1865 (1990); (b) H. Nakatsuji and S. Saito, Int. J. Quantum Chem. **39**, 93 (1991); (c) H. Nakatsuji, M. Sugimoto and S. Saito, Inorg. Chem. **29**, 3095 (1990).
[14] (a) H. Nakai, Y. Ohmori, and H. Nakatsuji, J. Chem. Phys. **95**, 8287 (1991); (b) H. Nakatsuji and M. Ehara, *ibid.* **97**, 2561 (1992); (c) K. Yasuda and H. Nakatsuji, *ibid.* **99**, 1945 (1993); (d) H. Nakai and H. Nakatsuji, J. Mol. Struct. (Theochem) **311**, 141 (1994); (e) S. Jitsuhiro, H. Nakai, M. Hada, and H. Nakatsuji, J. Chem. Phys. **101**, 1029 (1994); (f) H. Nakatsuji and M. Ehara, *ibid.* **101**, 7658 (1994); (g) H. Nakai, Y. Ohmori, and H. Nakatsuji, J. Phys. Chem. **99**, 8550 (1995).
[15] S. Huzinaga, J. Andzelm, M. Klobukowski, E. Radzio-Andzelm, Y. Sakai, and H. Tatewaki, *Gaussian Basis Sets for Molecular Calculations* (Elsevier, Amsterdam, 1984).
[16] MOTECC-91, M. Dupuis and A. Farazdel (Center for Scientific and Engineering Computations, IBM Corporation, 1991.)
[17] H. Nakatsuji, *Program System for the SAC/SAC-CI Calculations for Ground, Excited, Ionized, and Anion States of Molecules*, 1985, Program Library No. 146 (Y4SAC), Data Processing Center of Kyoto University; Program Library SAC85 (No. 1396), Computer Center of the Institute for Molecular Science, Okazaki.
[18] H. Nakatsuji, Chem. Phys. **75**, 425 (1983).
[19] L. Hedberg, T. Iijima, and K. Hedberg, J. Chem. Phys. **70**, 3224 (1979).
[20] GAUSSIAN92, M. J. Frisch, M. H. Gordon, G. W. Trucks, J. B. Foresman, H. B. Schlegel, K. Raghavachari, M. A. Robb, J. S. Binkley, C. Gonzarez, D. J. Defrees, D. J. Fox, R. A. Whiteside, R. Seeger, C. F. Melius, J. Baker, R. L. Martin, L. R. Kahn, J. J. P. Stewert, S. Topiol, and J. Pople (Gaussian, Inc., Pittsburgh, 1992).
[21] H. Jörg and N. Rösch, Chem. Phys. Lett. **120**, 359 (1985).
[22] C. W. Bauschlicher, Jr. and P. S. Bagus, J. Chem. Phys. **81**, 5889 (1984).
[23] I. A. Howard, G. W. Pratt, K. H. Johnson, and G. Dresselhaus, J. Chem. Phys. **74**, 3415 (1981).
[24] A. B. Rives and R. F. Fenske, J. Chem. Phys. **75**, 1293 (1981).
[25] (a) B. R. Henry and M. Kasha, Annu. Rev. Phys. Chem. **19**, 161 (1968); (b) M. Bixon and J. Jortner, J. Chem. Phys. **59**, 4061 (1969); (c) J. Jortner, S. A. Rice, and R. M. Hochstrasser, Advan. Photochem. **7**, 149 (1969), and references therein.
[26] F. J. Schlenker, F. Bouchard, I. M. Waller, and J. W. Hepburn, J. Chem. Phys. **93**, 7110 (1990).